3D Printing in Medicine

RESEARCH

Open Access

# Comparative analysis of conventionally and additively manufactured acetabular shells from a single manufacturer

Harry Hothi[1,2*], Johann Henckel[1], Arya Nicum[3], Anna Di Laura[1,2], Klaus Schlueter-Brust[4] and Alister Hart[1,3]

## Abstract

**Background** The Trident II Tritanium acetabular shell is additively manufactured (3D printed), based on the established Trident 'I' Tritanium shell, produced using conventional methods; this study characterised their differences.

**Methods** We obtained 5 Trident I (T1) and 5 Trident II (T2) shells sized 52 mm, 54 mm ($n=3$) and 60 mm. We measured their: mass, shell-liner engaging surface roughness, roundness, wall thickness, the depth of the bone-facing porous layer, porosity, and the number, volume and location of structural voids.

**Results** The mass varied by up to 13.44 g. The T1 and T2 shells had a median internal roughness of 0.18 µm and 0.43 µm, ($p<0.001$) and the median departure from roundness was 6.9 µm and 8.9 µm, ($p<0.001$). The 54 mm and 60 mm T2 shell walls were 37% and 29% thinner than their T1 counterparts ($p<0.01$). The T2 shells had irregular porous structures, shallower in depth by 11–27% ($p<0.001$) than T1 shells, which had repeating mesh units; the overall porosity was comparable (54%). All T2 shells had between 115 and 3415 structural voids, compared with two T1 shells containing 21 and 31 voids. There was no difference in the depth of the porous layer for the 54 mm T2 shells ($p=0.068$), whilst T1 shells did show variability ($p<0.01$). Both groups showed a variability in surface roughness and roundness ($p<0.01$).

**Conclusion** This is the first study to compare shells from a single manufacturer, produced using conventional and additive methods. This data will help interpret the performance of the 3D printed Trident II as longer-term clinical data is generated.

**Keywords** 3D-printing, Additive manufacturing, Acetabular shell, Micro-CT

*Correspondence:
Harry Hothi
harry.hothi@nhs.net
[1]The Royal National Orthopaedic Hospital, Stanmore HA7 4LP, UK
[2]The Department of Mechanical Engineering, University College London, London, UK
[3]The Institute of Orthopaedics and Musculoskeletal Science, University College London, London, UK
[4]Department of Orthopaedic Surgery, St. Franziskus Hospital Köln, 50825 Köln, Germany

## Background

The Trident Tritanium shell (Stryker, USA) is an example of a clinically successful acetabular shell used in total hip replacement surgery, with a risk of revision at 15 years of 4.05% [1]. The Tritanium coating is highly porous in its nature, offering the potential of enhanced bony fixation. It's conventional, subtractive manufacturing process consists of machining a solid titanium alloy to create the core shell substrate. The porous surface layer is created separately through a process which first creates a compacted meld of sacrificial particles, pure titanium particles and a polymeric binding agent. The sacrificial particles are then removed, leaving behind the desired pores and this structure is bonded to the underlying substrate through sintering processes. [2].

The Trident II Tritanium shell (Stryker, USA) is an entirely additively manufactured device which received FDA 510(k) clearance in 2016, based in part on the claim of substantial equivalence to the Trident Tritanium shell [3]. This utilises a process known as Selective Laser Melting (SLM) which uses a scanning laser beam to melt and fuse raw titanium powder to create the desired structure. The key manufacturing rationale of additively manufacturing (also referred to as 3D printing) the Trident II is the ability to reliably (1) produce a thinner walled shell, thereby allowing larger femoral head size options and (2) print complex, highly porous bone-facing surfaces to enhance long-term fixation [4]. The constraints of conventional methods places greater limits on the quality assurance of components at similar wall thicknesses and design complexities.


**Fig. 1** Macroscopic images showing an example of the two designs analysed: (**a** and **b**) the back and front sides of the Trident I shell and (**c** and **d**) the back and front sides of the Trident II shell

The clinical impact of the design changes in the Trident II will become clearer as long-term clinical and registry data is generated about its performance. Additive manufacturing is however a very different method of producing these shells compared with the conventional methods of the original Trident shell; this approach of 3D printing an implant, layer-by-layer, from a starting titanium powder has some known challenges, such as the risk of voids forming within the printed structure which may impact its mechanical properties [5].

Independent characterisation of the intended and unintended differences between these shells, produced by two different manufacturing methods, will help explain any differences in clinical performance that may occur in the future. The aim of this study was to characterise and compare the structural and morphometric properties of the Trident Tritanium and Trident II Tritanium shells, through analysis of final-production components of both designs.

## Methods

### Materials

This study examined 10 final-production, unused acetabular shells that had been produced by a single manufacturer (Stryker, Michigan, US). These consisted of (A) 5 Trident Tritanium Clusterhole Shells that had been conventionally manufactured from Ti6Al4V alloy and (B) 5 Trident II Tritanium Clusterhole Shells that had been 3D printed from a starting Ti6Al4V powder, Fig. 1. We obtained the same shell sizes for both groups: 52 mm ($n=1$), 54 mm ($n=3$) and 60 mm ($n=1$). From this point forward, the conventionally manufactured shells will be referred to as 'Trident I' and the 3D printed shells as 'Trident II'. The Trident I shells were assigned an identifier of *T1_52*, *T1_54_A*, *T1_54_B*, *T1_54_C* and *T1_60*. The Trident II shells were identified as *T2_52*, *T2_54_A*, *T2_54_B*, *T2_54_C* and *T2_60*.

The schematic in Fig. 2 summarises the analysis steps performed for the implants.

### Shell mass

The mass of each shell was measured using Mettler PC 4400 (Mettler Toledo, Leicester, United Kingdom) digital scales.

### Internal roughness

A Talyrond 365 (Taylor Hobson, Leicester, UK) was used to evaluate the roughness of the internal shell surface, at the shell-liner engagement interface, Fig. 2. A series of 5 vertical line traces were captured at 90° increments in each shell, using a 5 µm diamond stylus (20 traces per shell) and the Ra roughness measure was computed.

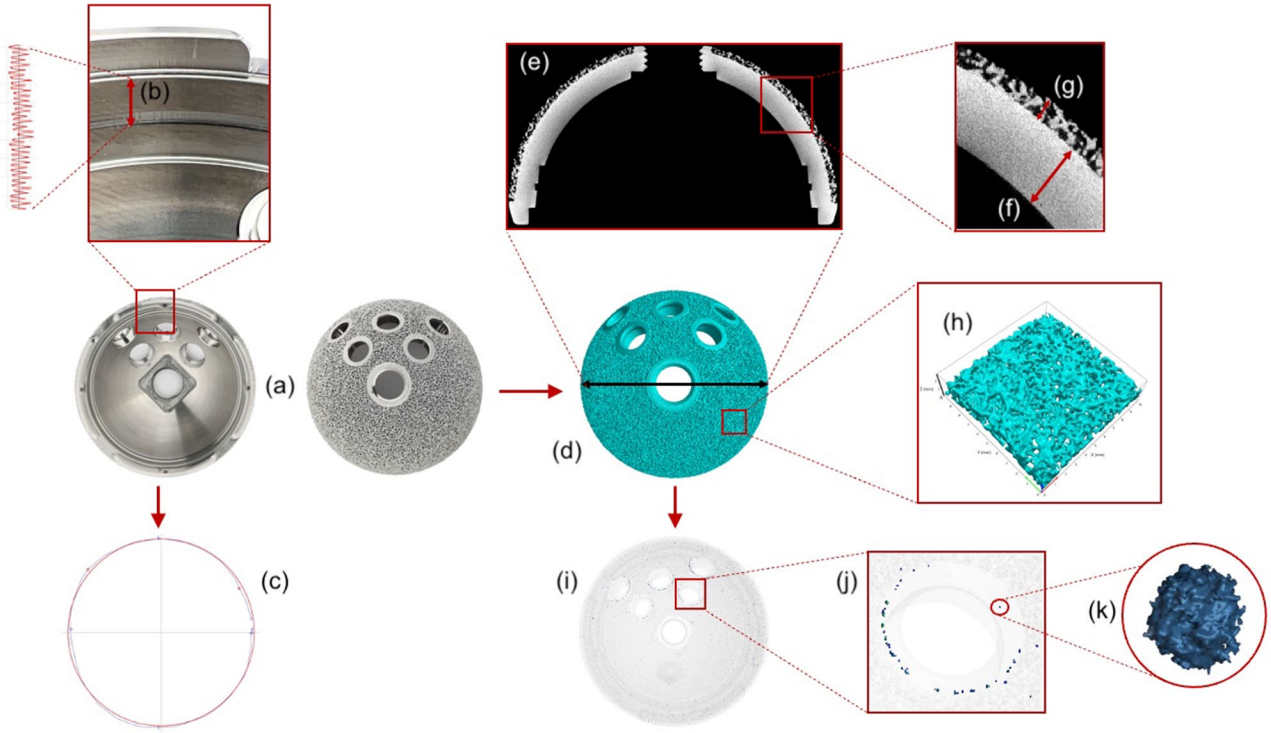


**Fig. 2** A schematic summary of the analysis steps performed using an example of (**a**) a Trident II shell. For each shell we (**b**) assessed the roughness of the internal shell-liner engagement surface, (**c**) determined the amount of any deviation from roundness of this engagement regions, (**d**) captured a 3D-micro-CT scan of the component and used this to (**e**) isolate 2D slices and (**f**) measure the thickness of the shell wall and (**g**) the depth of the porous layer. We then (**h**) analysed samples from the micro-CT scan to characterise the porous structure, with measures of strut thickness, pore size and the amount of porosity. The whole micro-CT scan data was used to (**i**) determine the presence of any voids, (**j**) determine the location of these and (**k**) determine the volume and size of these

### Shell roundness

A Zeiss Contura (Carl Zeiss, Rugby, UK) coordinate measurement machine (CMM) was then used to determine the roundness of the shell-liner engagement region. A 2 mm ruby stylus was used to capture 10 circular traces which were analysed in accordance with ISO 1101, to determine the separation of two concentric circles fitted within and outside of the captured traces; a lower separation indicates a smaller departure from roundness.

### Micro-CT imaging

A Nikon XTH 225 micro-CT scanner (Nikon Metrology, Tring, United Kingdom) was used to capture high resolution 3D images of each shell. Scans were performed with a beam current and voltage of up to 110 μA and 225 kV respectively. A 2.0 mm thick copper filter was fitted in front of the beam source in order to minimise any beam hardening induced when scanning a metal sample. The two-dimensional (2D) projection images were first reconstructed in CT Pro 3D software (Nikon Metrology, UK), whilst applying a filtered back-projection algorithm. Second-order polynomial-correction numerical filtering was also applied within the algorithm to further minimise any beam hardening that may have occurred. The spatial resolution of the images for analysis was 0.09 mm; the voxel size of the scans was 0.045 mm.

### Shell volume

The filtered and corrected micro-CT data was imported into the analysis software package Volume Graphics (Heidelberg, Germany) and the shells were segmented using an ISO-50 approach. An automated calculation of the volume of each shell was then obtained.

### Morphometric analysis of micro-CT data

The micro-CT data was then analysed using Volume Graphics and Simpleware (Synopsis, Exeter, UK) in order to measure (1) the wall thickness of the dense regions of the shells, (2) the depth of the porous layers, (3) the strut thickness of the porous structures, (4) the pore size and (5) the level of porosity.

### Shell wall thickness

2D projection images from the scans were examined in Simpleware after applying a multi-Otsu thresholding algorithm to separate the titanium implant from the background (air). The 2D image bisecting each shell was

selected and 5 measures of the thickness of the dense region of each shell were obtained.

#### Porous layer depth

The same 2D projection images were then examined to capture 5 measures of the thickness of the porous layers on each shell.

#### Strut thickness measurement

A multi-Otsu thresholding algorithm was applied in Simpleware to separate the titanium implant from the background (air) and render a segmented 3D model of each cup. A sphere was best fit to the transition between the porous and dense regions of the implants. Through Boolean subtraction, the porous layer was isolated from the rest of the implant using the defined sphere. Five samples of the porous structures within the main cup body were captured computationally for analysis, measuring 10×10 mm in length and width and including the entire depth of the porous layer. A wall thickness function within Simpleware allowed the mean thickness of the struts to be recorded in each sample.

#### Pore size measurement

With respect to the Trident I, the pore size of the mesh structure of each sample was measured by best fitting a sphere to the internal surface of a single mesh unit. This was performed on five unique units within each sample.

The Trident II did not have a single, repeating mesh unit and the pore shape was more irregular in nature; a best fitting sphere method was therefore not suitable and so a different approach was adopted. This necessitated manual measurement of the distance between struts to determine the pore size at different regions. This was achieved by (1) identifying and isolating adjacent struts and then (2) inverting the mesh so as to allow the space between the struts to be measured using a wall thickness operation.

#### Porosity measurement

The previously isolated regions within the captured samples were used to determine the level of their porosity, expressed as a percentage, of the volume of this region relative to the volume of the mesh material within this space.

#### Void analysis

The Porosity/Inclusion Analysis module within the Volume Graphics software was then used to investigate the presence of any voids within the components, that may indicate structural defects. The VGDefX algorithm was applied during analysis, in which variations in grey scale values are assessed and compared for each voxel of the scan to determine if the voxel forms part of a void or of the material. An edge distance calculation was performed for each void that was identified, in order to determine the minimum distance between the void and the surface of the implant. Following this analysis, the following parameters were obtained for each shell:

(1) The number of voids/mm$^3$.
(2) The total volume of voids and the shell volume fraction.
(3) The size of each void.
(4) The distance of each void from the shell surface.

#### Statistical analysis

We performed Mann-Whitney U tests to determine if there were any significant differences in the parameters investigated between the two shell designs (where applicable). Kruskal-Wallis tests were used to identify if there were any significant differences between shells of the same 54 mm size in the groups, with Dunn's multiple comparisons tests used for post-hoc analysis. All analysis was performed using the statistical software package Prism (GraphPad, La Jolla, California) and throughout, a p-value $<0.05$ was considered statistically significant.

## Results

#### Shell mass

The mass of each shell (mean of the three readings) is presented in Table 1. The 52 mm and 60 mm sizes of the T1 shells were heavier than their T2 equivalents by 13.23 g and 13.44 g respectively. Conversely, the 54 mm T2 shells were approximately 10 g heavier than the 54 mm T1 shells. The three 54 mm T1 shells had a difference of 0.15 g between their mass measurements; the three 54 mm T2 shells had a difference of 0.95 g. Shell T2_54_B was 0.25 g lighter than T2_54_A, whilst shell T2_54_C was 0.95 g lighter than T2_54_A.

#### Internal roughness

The roughness measures of the internal surface of each shell are presented in Fig. 3. T1 and T2 shells had a median Ra of 0.18 μm (0.12–0.36) and 0.43 μm (0.37–0.55) respectively; this difference was statistically significant ($p<0.001$). Kruskal-Wallis analysis of the three 54 mm T1 shells indicated significant differences between their median Ra values ($p<0.001$); post-hoc analysis showed T1_54_B to have a greater roughness than the other two cups. Kruskal-Wallis analysis of the three 54 mm T2 shells also revealed differences ($p=0.019$), such that the roughness of T2_54_C was greater than T2_54_B ($p=0.015$).

**Table 1** Summary of the defect analysis data obtained for each shell, detailing the presence and characteristics of structural voids. Measures of the volume, mass and density are also presented

| Shell | Volume ($cm^3$) | Mass (g) | Density ($g/cm^3$) | Number of Voids | Total Volume of Voids ($mm^3$) | Void Concentration ($voids/mm^3$) | Volume Fraction (%) | Median (range) Void Sphericity | Median (range) Void Size (mm) | Median (range) Distance of Voids from surface (mm) |
|---|---|---|---|---|---|---|---|---|---|---|
| T1_52 | 14.17 | 62.15 | 4.39 | 0 | 0.00 | 0.000 | 100.00 | - | - | - |
| T2_52 | 11.41 | 48.77 | 4.27 | 1315 | 0.88 | 0.115 | 99.99 | 0.52 (0.27–0.66) | 0.16 (0.10–0.72) | 0.29 (0.05–1.25) |
| T1_54_A | 13.72 | 58.64 | 4.27 | 0 | 0.00 | 0.000 | 100.00 | - | - | - |
| T1_54_B | 13.97 | 58.49 | 4.19 | 0 | 0.00 | 0.000 | 100.00 | - | - | - |
| T1_54_C | 13.68 | 58.60 | 4.28 | 21 | 0.01 | 0.002 | 100.00 | 0.56 (0.5–0.62) | 0.15 (0.13–0.22) | 0.50 (0.21–1.16) |
| T2_54_A | 16.35 | 68.65 | 4.20 | 455 | 1.05 | 0.028 | 100.00 | 0.54 (0.34–0.72) | 0.24 (0.12–0.96) | 0.20 (0.07–1.4) |
| T2_54_B | 16.40 | 68.40 | 4.17 | 3415 | 4.76 | 0.208 | 99.97 | 0.52 (0.27–0.69) | 0.22 (0.11–0.87) | 0.31 (0.06–1.84) |
| T2_54_C | 15.79 | 67.70 | 4.29 | 800 | 1.21 | 0.051 | 99.99 | 0.52 (0.28–0.68) | 0.21 (0.12–0.86) | 0.24 (0.06–1.74) |
| T1_60 | 22.72 | 91.01 | 4.01 | 31 | 0.02 | 0.150 | 100.00 | 0.53 (0.18–0.46) | 0.21 (0.15–0.27) | 0.95 (0.30–1.49) |
| T2_60 | 18.70 | 77.57 | 4.15 | 115 | 0.27 | 0.006 | 100.00 | 0.52 (0.33–0.66) | 0.25 (0.13–0.75) | 0.25 (0.09–1.22) |

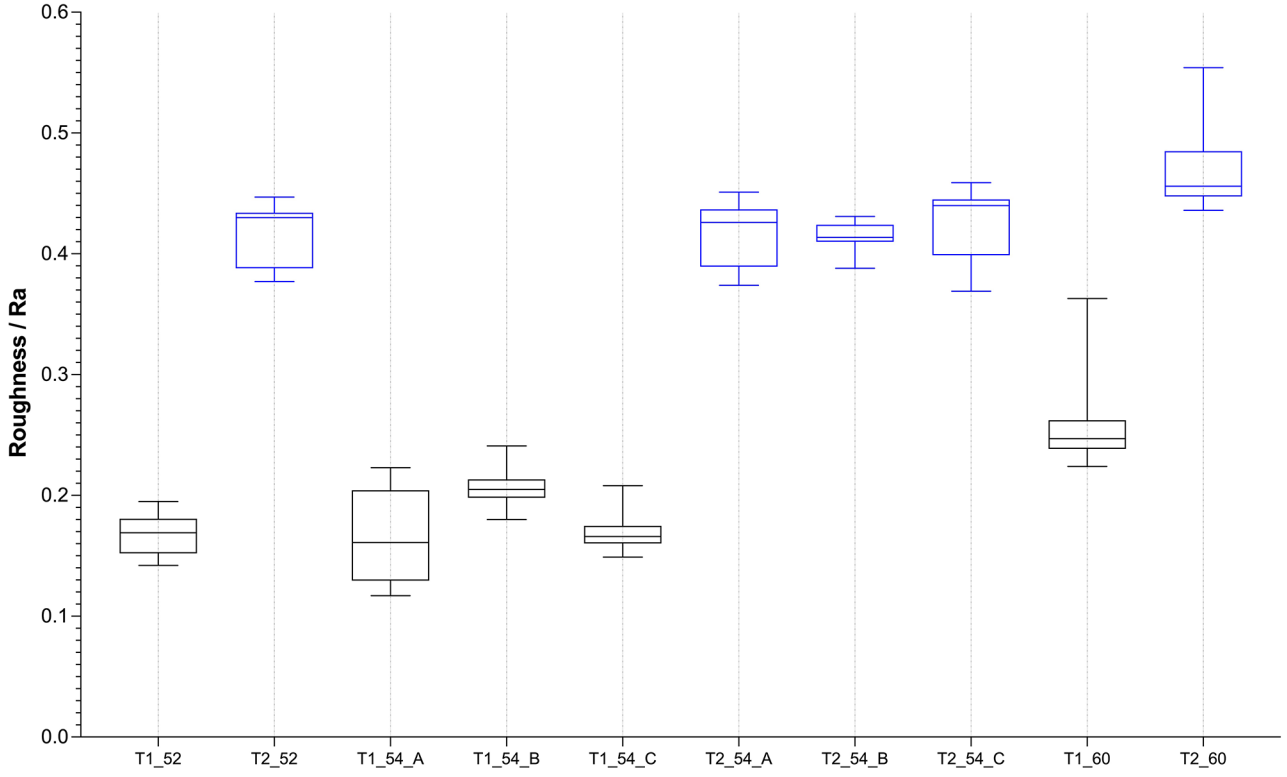


**Fig. 3** Box-plots of the measures of surface roughness obtained on the internal surface of each shell at the shell-liner engagement point

### Shell roundness

The T1 and T2 shells had a median departure from roundness of 6.9 μm (4.2–10.8) and 8.9 μm (5.0-16.1) respectively; this difference was significant ($p<0.001$). Kruskal-Wallis analysis revealed a variability between the three 54 mm T1 shells ($p=0.0019$); post-hoc analysis showed that T1_54_C had a greater deviation from roundness from T1_54_A ($p=0.0021$) and T1_54_B ($p=0.0317$).

There was also a variability between the three 54 mm T2 shells ($p=0.0074$); T2_54_C had a smaller departure from roundness than shells T2_54_A ($p=0.0255$) and T2_54_B ($p=0.0161$).

### Shell volume

Table 1 presents the computed shell volumes. The three 54 mm T1 shells varied by $0.29mm^3$ and were smaller in volume than the 54 mm T2 shells. Shell T2_54_C was $0.61mm^3$ smaller in volume than the shells T2_54_A and T2_54_B, which differed by $0.05mm^3$.

### Shell wall thickness

Figure 4 presents box plots of the wall thickness measures of the shells. Shells T1_52 and T2_52 had median wall thicknesses of 4.33 mm (3.96–4.44) and 2.73 mm (2.66–2.89) respectively; this difference was significant ($p=0.0079$). Shells T1_60 and T2_60 had median wall thicknesses of 4.51 mm (4.15–4.55) and 3.18 (3.15–3.28) respectively; this difference was significant ($p=0.0079$).

The median thickness of the 54 mm T 1 and T 2 shells was 3.45 (2.91–3.55) and 3.80 mm (3.42–3.86) respectively; this difference was significant ($p<0.001$). Kruskal-Wallis analysis revealed no difference between the three 54 mm T1 shells ($p=0.551$) and the three 54 mm T2 shells ($p=0.808$).

### Porous layer depth

Shells T1_52 and T2_52 had median porous depths of 1.50 mm (1.13–1.57) and 1.34 mm (0.99–1.32) respectively; this difference was significant ($p<0.001$). Shells T1_60 and T2_60 had median porous depths of 1.47 mm (1.01–1.70) and 1.08 mm (0.95–1.37) respectively; this difference was significant ($p<0.001$).

The median depths of the 54 mm T1 and T2 shells was 1.49 mm (1.32–1.90) and 1.12 mm (0.82–1.33) respectively; this difference was significant ($p<0.001$). Kruskal-Wallis analysis revealed a difference between the three 54 mm T1 shells ($p=0.0046$); post-hoc analysis showed that the T1_54_A shell had a significantly greater depth than T1_54_B ($p=0.011$) and T1_54_C ($p=0.017$). There was no difference between the three 54 mm T2 shells ($p=0.0684$).

### Strut thickness measurement

The T1 and T2 shells had a median strut thickness of 0.29 mm (0.26–0.34) and 0.36 mm (0.31–0.42) respectively; this difference was significant ($p<0.001$). Kruskal-Wallis analysis revealed no difference between the three 54 mm T1 shells ($p=0.794$) but a difference between the three 54 mm T2 shells ($p<0.001$). Post-hoc analysis revealed that the struts of shell T2_54_C were significantly narrower than shell T2_54_A ($p=0.0012$).

### Pore size measurement

The T1 and T2 shells had a median pore size of 0.66 mm (0.50–0.91) and 0.36 mm (0.33–0.40) respectively; this difference was significant ($p<0.001$). Kruskal-Wallis analysis revealed no difference between the three 54 mm T1 shells ($p=0.9680$) or the three 54 mm T2 shells ($p=0.1015$).

### Porosity measurement

The samples from the T1 and T2 shells had a median porosity of 54.09% (46.13-59.00) and 53.48% (46.61–59.87) respectively; there was no difference between the

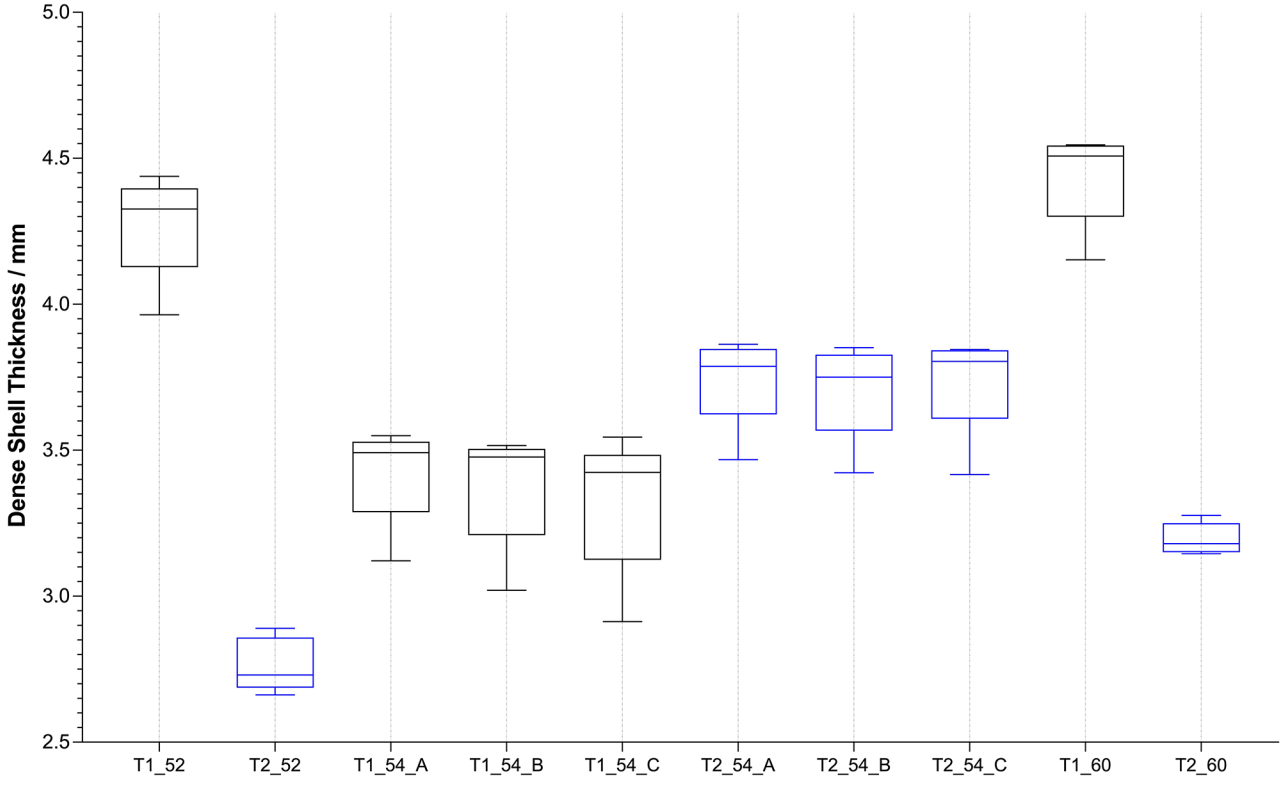


**Fig. 4** Box-plots of the measures of the thickness of the dense wall structures of each shell

two groups ($p=0.606$). The T1 shells had porous layers consisting of repeating units, whilst the T2 shells had an irregular structure, Fig. 5.

### Number of voids

The void analysis parameters obtained are summarised in Table 1. Three of the five T1 shells appeared to have no evidence of voids. Shells T1_54_C and T1_60 had 21 and 31 voids respectively. All T2 shells had evidence of voids, with a median number of 800 (115–3415).

### Void volume

The voids in the two T1 shells occupied a total volume of 0.01 and 0.02 $mm^3$. The resulting volume fraction in both cases remained at 100% at 5 decimal places. The voids in the T2 shells occupied a median volume of 1.05 $mm^3$ (0.27–4.76), with a resulting volume fraction of 99.99% (99.97–100).

### Void size

The voids in the T1 and T2 shells had a median diametrical size of 0.19 mm (0.13–0.27) and 0.29 mm (0.12–0.65) respectively; this difference was significant ($p<0.001$).

### Void location

The voids in the T1 and T2 shells were located a median of 0.85 mm (0.25–1.49) and 0.20 mm (0.07–1.53) from their surfaces; this difference was significant ($p<0.001$). Figure 6 presents an example of the location of voids in one of the T1 shells, which were distributed across the dense region of the shell body. Figure 7 presents an example of the location of voids in one of the T2 shells, which were also distributed within dense regions. There were clusters of voids located around all screw holes and isolated voids around the central introducer hole. Voids were also found to exist circumferentially in the vicinity of the shell rim.

## Discussion

This is the first study to perform comparative analysis between conventional and additive manufactured acetabular shells designs from a single manufacturer. The 3D printed Trident II shells of the same size were consistent in their dimensional measures, whereas the equivalent Trident I shells, that were manufactured using conventional subtractive methods, demonstrated some variability in their porous layers. The Trident II shells however were found to contain considerably more structural voids than their Trident I counterparts. This study provides further data that may help interpret any differences in clinical performance as longer term clinical and registry data is generated; these may relate to the extent of bony integration and fixation, as well as the potential of fracture due to the presence of structural cavities in the T2 shells.

The differences in the mass of the shells corresponds with the differences in their wall thicknesses. The 52 and 60 mm sizes of the Trident II shells were lighter than their corresponding Trident I shells but also had thinner walls, whilst the heavier 54 mm Trident II shells had thicker walls. The thinner wall of the 52 mm T2 shell in particular demonstrates one of the advantages of 3D printing; this design will enable a larger head size to be used compared with when a 52 mm T1 shell is used, without removing any additional bone stock. This T2 shell wall was 37% thinner than it's equivalent T1 design and consequently is able to accommodate a maximum

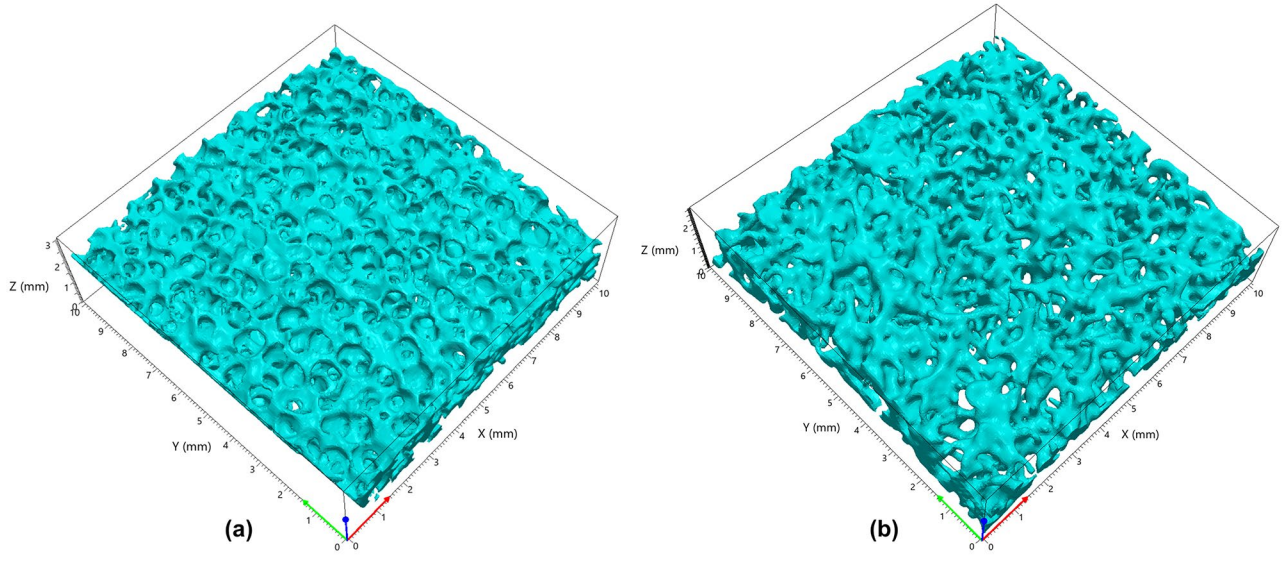


**Fig. 5** Samples of the porous regions of the (**a**) Trident I and (**b**) Trident II shells

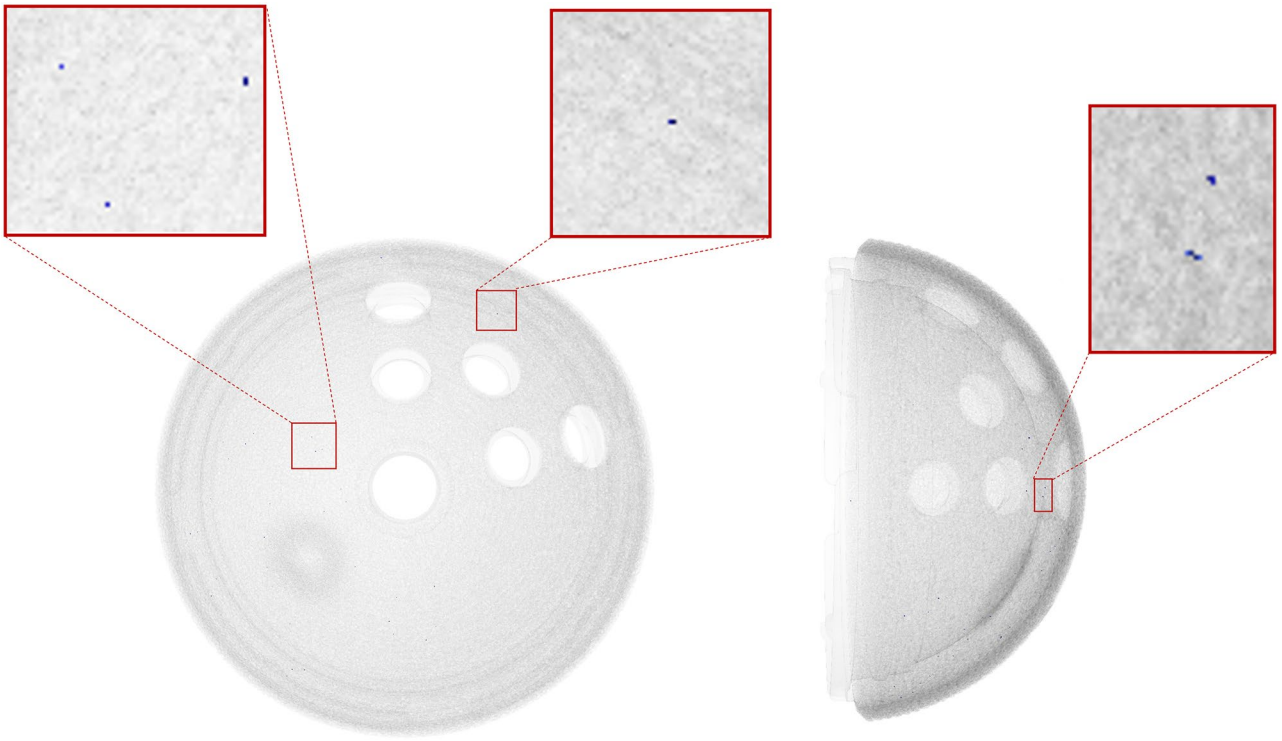

**Fig. 6** An example of two views of a Trident I shell, showing the presence of structural voids

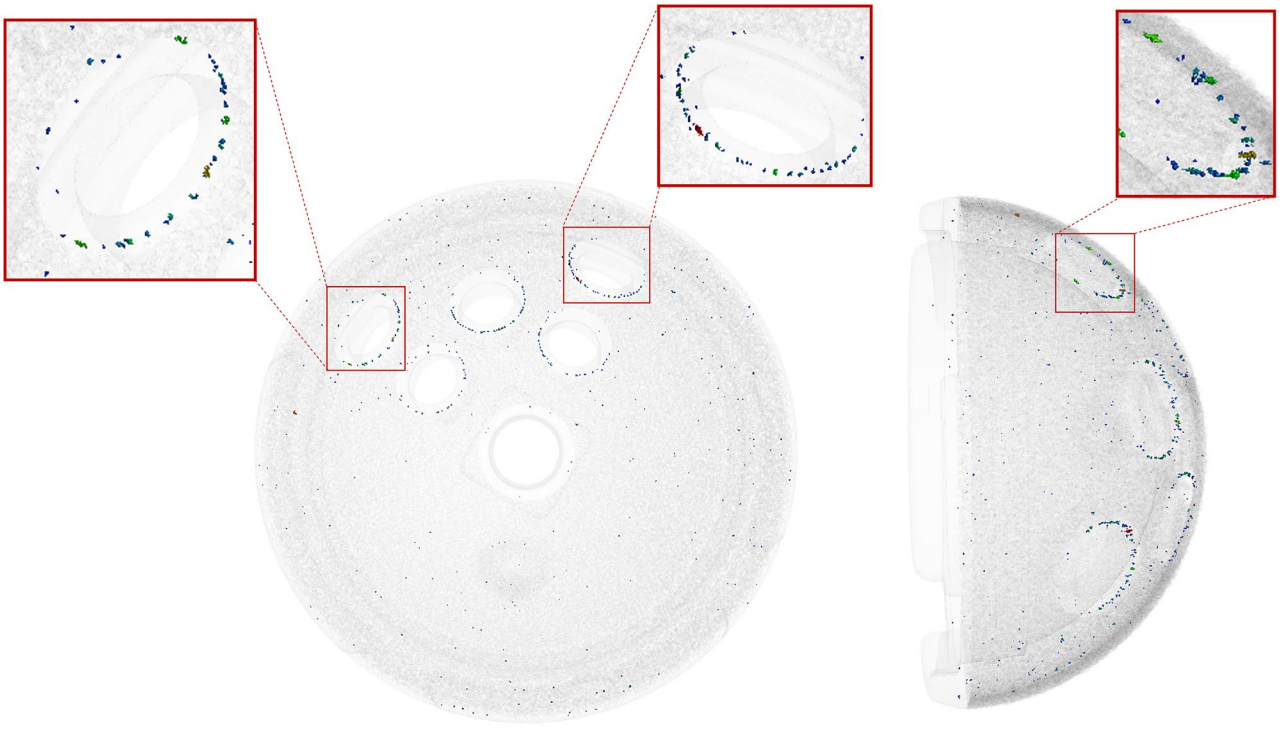

**Fig. 7** An example of two views of a Trident II shell, showing the presence of structural voids

femoral head size of 40 mm, compared with a maximum head size of 36 mm in a 52 mm T1 shell [4, 6].

The median roughness of the internal shell-liner engagement surface of the T2 components was approximately twice that of the T1 shells. These differences may be due to any differences that may exist in the post-processing methods and machinery used between the two designs, may be an indicator of a greater difficulty in polishing 3D printed parts, or indeed may be due to a variability in the printing process itself. The median Ra measures of both the T1 (0.18 μm) and T2 (0.43 μm) shells were however less than those reported for other comparable shell designs, which have known Ra measures of up to 4 μm [7, 8]. This is reassuring given evidence in literature indicating an increased risk of backside wear in polyethylene liners when paired against titanium shells with rougher engaging surfaces, close to Ra measures of 4 μm [7, 8]. Similarly, the departure from roundness of the T2 shells was statistically greater than in the T1 shells however both designs were within manufacturing tolerances expected for this type of component [9].

The Food and Drug Administration (FDA) had previously issued 510(k) approval that the T2 shells were substantially equivalent to T1 shells. This was determined using laboratory testing which include push-, lever- and torque-out tests, as well as tests of fatigue, plastic deformation, material chemistry and characterisation of the porous surface. The methods presented in the current study build on our previous research investigating AM implants, particularly with the use of micro-CT, and adds further data to the similarities and differences between the AM and conventionally manufactured designs.

Interestingly, we measured the 3D printed T2 shells as having a shallower bone-facing porous layer than their equivalently sized T1 shells. With the median depth ranging between 1.47 and 1.50 mm and 1.08–1.34 mm for the T1 and T2 shells respectively, both designs were within a depth of 2.5 mm, which has previously been suggested as being the maximum depth to which bone can grow in porous structures [10]. Conversely, it is not yet clear in literature what the minimum porous depth should be to ensure sufficient bone growth for long-term bony fixation. The Delta TT shell (LimaCorporate, Italy) has a reported porous structure depth of between 1.28 and 1.47 mm and has demonstrated very good long-term clinical success, rated 10 A* by the UK Orthopaedic Device Evaluation Panel (ODEP) [11, 12]. Longer term clinical data will help understanding of impact of the shallower porous layer of the Trident II with respect to bone growth. We found that the porosity however of the bone-facing structures of both shell designs was comparable, at approximately 54%. The Trident I porous structure was composed of repeating mesh units, whilst the structure of the Trident II porous layer was irregular in its nature, with differing strut thicknesses and pore sizes; the manufacturer describes this irregularity as mimicking the structural characteristics of cancellous bone [4]. We do not currently know the optimal porous design to use in orthopaedic implants to maximise bone ingrowth, or indeed if a single optimal design exists. A key factor that will influence bone in-growth is the shape and size of the pores within these structures (i.e., the available space between the struts for bone to grow into). Previous studies have suggested a broad range of optimal pore sizes of between 100 μm and greater than 1000 μm, and similarly have reported advantages in using either repeating or irregular lattice structures [13–18]. As stated previously, the clinical advantages, if any, of utilising an irregular porous mesh in the Trident II rather than the repeating structure of the Trident I will become clearer through long term outcome data.

There was evidence of structural voids within all Trident II shells in this study and in two of the Trident I shells. The impact of the low number of isolated voids on the resulting volume fraction in the Trident I shells appears to be negligible, with both calculated as 100% at 5 decimal places. Similarly, the lowest volume fraction in the Trident II shells was 99.97% in a shell with 3415 voids. The presence of voids in all of Trident II shells is unsurprising as this is a known occurrence in additive manufacturing, and has been reported in other shell designs [5]. All manufacturers carry out post-processing in order to eliminate these voids, most commonly through a process of hot isostatic pressing (HIP) [19]. It has been reported however that these methods may be less effective in fully removing voids situated close to component surfaces [20]; this appears consistent with the location of voids in the Trident II shells, which were within a median of 0.20 from their surfaces. Interestingly, the majority of voids in these shells were situated around the periphery of screw holes, which may be due to the change in shape in these regions for the printer to adjust to. We do not know the impact of these voids on the structural integrity of the shells. Evidence from testing of 3D printed titanium parts within the aerospace industry has suggested that high cycle loading of components with voids may eventually lead to the formation of fatigue cracks, particularly if these voids are located close to the surface [21]. There is however no evidence of a fracture of this design of 3D printed shell having occurred, or indeed of any 3D printed orthopaedic shell which are also known to contain structural voids.

Obtaining three shells of the same size for both designs offered an opportunity to provide preliminary data on the potential variability in the two manufacturing methods. The Trident II shells appeared to have greater variability in their mass and volume compared with the Trident

I shells however this difference was comparatively very small. Additionally, the Trident I shells were found to have a statistically significant variability in (1) the internal roughness, (2) roundness, and (3) porous layer depth. The Trident II shells also showed variability in their internal roughness and roundness measures however were consistent with porous depth. We also found some variability in the strut thickness measurements between the three 54 mm Trident II shells however this is unsurprising given the irregular porous mesh design used. It is difficult at this stage to separate out the source of the variability observed within both shell designs; it may be such that it is due to a combination of inconsistencies introduced both during the manufacturing stage and during post-processing.

We acknowledge the relatively small sample size as a limitation of this study. The data presented here however provides surgeons and researchers with an understanding of the key differences between these two designs manufactured using very different methods. Future studies involving a greater number of samples will help clarify the extent of manufacturing variability, for example in the measurement of mass and volume. Additionally, future research involving mechanical testing and finite element analysis of these shells will help understanding of the impact of any differences on their mechanical properties. Destructive testing may also enable further characterisation of the microstructure of these components, including the grain size and orientation.

## Conclusions

This is the first study to perform comparative analysis between the Trident I and Trident II shells, which had been manufactured using conventional and additive (3D printed) methods respectively. We have characterised the differences between the two designs in their mass, wall thickness, porous structure design and depth, as well as the surface finish and roundness of the shell-liner interface. There was no difference in the dimensional properties of the 3D printed Trident II shells of the same size, however there was variability in the porous layer within the equivalent Trident I shells. Both designs demonstrated a variability in their surface finish and roundness. The wide range of structural voids observed in the Trident II shells may point to challenges in both the printing process itself and the post-processing methods used to eliminate these. This study provides data to help interpret clinical performance as longer term clinical and registry data is generated.

**Acknowledgements**
We acknowledge the support of The Arthroplasty for Arthritis Charity, the Maurice Hatter Foundation, the RNOH Charity, the Rosetrees Trust and the Stoneygate Trust, and by researchers at the National Institute for Health Research, University College London Hospitals Biomedical Research Centre.

**Author contributions**
HH, JH, AH. Study Design: HH, JH, AN, AH. Data Acquisition: HH, ADL, KSB. Interpretation of Data: HH, JH, ADL, KSB, AH. Manuscript writing and/or revision: HH, JH, AN, ADL, KSB. AH. All authors read and approved the final manuscript.

**Funding**
This research did not receive any specific grant from funding agencies in the public, commercial, or not-for-profit sectors.

**Data availability**
No datasets were generated or analysed during the current study.

## Declarations

**Ethics approval and consent to participate**
Not applicable.

**Consent for publication**
Not applicable.

**Competing interests**
The authors declare no competing interests.

Received: 22 April 2024 / Accepted: 5 August 2024
Published online: 29 September 2024

**References**

1. The National Joint Registry. NJR 19th Annual Report. 2022. https://reports.njrcentre.org.uk
2. Muth J, Poggie M, Kulesha G, et al. Novel highly porous Metal Technology in Artificial hip and knee replacement: Processing methodologies and clinical applications. JOM. 2013;65:318–25.
3. Food and Drug Administration. 510(k) Premarket Notification of Trident II Tritanium Acetabular Shells. 2016. https://www.accessdata.fda.gov/cdrh_docs/pdf16/K161569.pdf
4. Stryker. Trident II Acetabular System Design Rationale. 2019. http://az621074.vo.msecnd.net/syk-mobile-content-cdn/global-content-system/SYKGCS-DOC-2-46752/z9HnY9HGqa_jUaAq1N7McKVPwOJ9XQ/TRIDII_SS_1.pdf
5. Hothi H, Dall'Ava L, Henckel J, Di Laura A, Iacoviello F, Shearing P, Hart A. Evidence of structural cavities in 3D printed acetabular cups for total hip arthroplasty. J Biomed Mater Res B Appl Biomater. 2020. Jul;108(5):1779–89.
6. Stryker. Tritanium Acetabular System Surgical Protocol. 2010. https://surgeryadvisor.files.wordpress.com/2016/02/trident-tritanium-revision-tecnica-op.pdf
7. Braun S, Sonntag R, Schroeder S, Mueller U, Jaeger S, Gotterbarm T, Kretzer JP. Backside wear in acetabular hip joint replacement. Acta Biomater. 2019;83:467–76.
8. Braun S, Vardag S, Mueller U, Schroeder S, Sonntag R, Bormann T, Gotterbarm T, Kretzer JP. Backside wear, particle migration and effectiveness of screw hole plugs in acetabular hip joint replacement with cross-linked polyethylene. Acta Biomater. 2019;97:239–46.
9. Heisel C, Kleinhans JA, Menge M, Kretzer JP. Ten different hip resurfacing systems: biomechanical analysis of design and material properties. Int Orthop. 2009. Aug;33(4):939–43.
10. Li JP, Habibovic P, van den Doel M, Wilson CE, de Wijn JR, van Blitterswijk CA, de Groot K. Bone ingrowth in porous titanium implants produced by 3D fiber deposition. Biomaterials. 2007;28(18):2810–20.
11. Dall'Ava L, Hothi H, Henckel J, Di Laura A, Shearing P, Hart A. Comparative analysis of current 3D printed acetabular titanium implants. 3D print Med. 2019. Nov 6;5(1):15.
12. Orthopaedic Device Evaluation Panel (ODEP). Delta TT Acetabular Cup. 2021. https://www.odep.org.uk/product/delta-tt-acetabular/
13. Boyan BD, Hummert TW, Dean DD, Schwartz Z. Role of material surfaces in regulating bone and cartilage cell response. Biomaterials. 1996;17(2):137–46.
14. Freyman TM, Yannas IV, Gibson LJ. Cellular materials as porous scaffolds for tissue engineering. Prog Mater Sci. 2001;46:273e82.
15. Li G, Wang L, Pan W, et al. In vitro and in vivo study of additive manufactured porous Ti6Al4V scaffolds for repairing bone defects. Sci Rep. 2016;6:34072.

16. Kujala S, Ryhänen J, Danilov A, Tuukkanen J. Effect of porosity on the osteointegration and bone ingrowth of a weight-bearing nickel-titanium bone graft substitute. Biomaterials. 2003;24(25):4691–7.
17. Frosch KH, Barvencik F, Viereck V, Lohmann CH, Dresing K, Breme J, Brunner E, Stürmer KM. Growth behavior, matrix production, and gene expression of human osteoblasts in defined cylindrical titanium channels. J Biomed Mater Res A. 2004;68(2):325–34.
18. Zhao D, Huang Y, Ao Y, Han C, Wang Q, Li Y, Liu J, Wei Q, Zhang Z. Effect of pore geometry on the fatigue properties and cell affinity of porous titanium scaffolds fabricated by selective laser melting. J Mech Behav Biomedical Mater. 2018;88:478–87.
19. Tammas-Williams S, Withers PJ, Todd I, Prangnell PB. The effectiveness of hot isostatic pressing for closing porosity in titanium parts manufactured by selective electron beam melting. Metall Mater Trans Phys Metall Mater Sci. 2016;47:1939–46.
20. Du Plessis A, Yadroitsava I, Yadroitsev I. Effects of defects on mechanical properties in metal additive manufacturing: a review focusing on X-ray tomography insights. Mater Des. 2020;187:1–19.
21. Benedetti M, Fontanari V, Bandini M, Zanini F, Carmignato S. Low- and high- cycle fatigue resistance of Ti-6Al-4V ELI additively manufactured via selective laser melting: mean stress and defect sensitivity. Int J Fatigue. 2018;107:96–109.

## Publisher's Note